Proteomic Analysis of Early Response Lymph Node Proteins in Mice Treated with Titanium Dioxide Nanoparticles

Yuan Gao[1], **Neera V. Gopee**[2], **Paul C. Howard**[3], and **Li-Rong Yu**[1,*]

[1]Center of Excellence for Proteomics, Division of Systems Biology, National Center for Toxicological Research, FDA, Jefferson, AR 72079, USA

[2]Division of Veterinary Services, National Center for Toxicological Research, FDA, Jefferson, AR 72079, USA

[3]Division of Biochemical Toxicology and Office of Scientific Coordination, National Center for Toxicological Research, FDA, Jefferson, AR 72079, USA

Abstract

Human exposure to nanoparticles is inevitable from natural and anthropogenic sources. Titanium dioxide (TiO_2) nanoparticles are increasingly being used in pharmaceutical and cosmetic products. Previous studies revealed that TiO_2 levels were significantly increased in tissues (e.g., lymph nodes) after mice were injected with nanosized TiO_2. To identify early response lymph node proteins to TiO_2 nanoparticles, groups of mice were intradermally injected with a low dose of DeGussa P25 TiO_2 nanoparticles or vehicle alone. The proteomes of lymph nodes at 24 h were quantitatively analyzed using trypsin-catalyzed $^{16}O/^{18}O$ labeling in conjunction with two-dimensional liquid chromatography separation and tandem mass spectrometry (2DLC-MS/MS). A total of 33 proteins were significantly changed (over 1.3-fold, $p<0.05$) in the mice treated with TiO_2 nanoparticles, which accounted for approximately 1% of the total proteins identified. The differentially expressed proteins mainly involve the immune response (e.g., inflammation), lipid and fatty acid metabolism, mRNA processing, and nucleosome assembly. Regulation of functionally distinct classes of proteins could be mediated by estrogen receptor (ESR1), PPARγ, and c-Myc signalings, etc. The differentially expressed proteins identified in this experiment could represent early response proteins to TiO_2 nanoparticle treatment in mouse lymph nodes.

Keywords

proteomics; mass spectrometry; TiO_2 nanoparticle; mouse lymph node; $^{16}O/^{18}O$ labeling; LC-MS/MS

1. Introduction

Nanoparticles are typically defined as particles with at least one size domain between 1 and 100 nanometers. Engineered nanoparticles have emerged as a class of new materials for more than a decade. The unique characteristics of some materials in this size domain and

*Address correspondence to: Dr. Li-Rong Yu, Center of Excellence for Proteomics, Division of Systems Biology, National Center for Toxicological Research, U.S. Food and Drug Administration, 3900 NCTR Rd., HFT-233, Jefferson, AR 72079, USA. Phone: 870-543-7052; Fax: 870-543-7686; Lirong.Yu@fda.hhs.gov or Paul.Howard@fda.hhs.gov.

various applications of nanomaterials are attractive for commercial development. Studies have indicated that nanomaterials are used in many daily consumed products such as beer and baby drinks despite the limited safety information that has been acquired (1). So far, more than 1300 nanotechnology-based consumer products, produced by ~580 companies located in 30 countries have been reported (http://www.nanotechproject.org/inventories/consumer/). Several pharmaceutical companies already obtained approval from the U.S. Food and Drug Administration (FDA) for medical applications of nanotechnology-based drug-delivery agents, biosensors, and imaging contrast agents (2, 3). While the types of nanoparticles and applications continue to grow, concerns are mounting for the health risk of human exposure to nanomaterials (4-9). Therefore, *in vivo* studies to characterize biological responses to nanomaterial exposure are in growing need (10).

Among the commercially available nanomaterials, titanium dioxide (TiO_2) nanoparticles are increasingly being used in personal care, paint, cosmetic products and food additives (http://www.nanotechproject.org/inventories/consumer/). Possible approaches of human intake of TiO_2 nanoparticles include airborne exposure, inhalation, ingestion, skin uptake, and medical injection of engineered nanomaterials (11, 12). The uptake of nanomaterials in tissues will be dependent on the site of interaction of the nanomaterials with the organism. Intravenous injection of TiO_2 nanoparticles in mice/rats resulted in elevated TiO_2 levels in blood and solid tissues (13) with the highest TiO_2 levels found in liver, followed by blood, spleen, lung, and kidney (13, 14) one day after the treatment. In contrast, intradermally injected nanoparticles (e.g., cadmium selenide quantum dots) were taken up by lymph nodes and translocated to the blood stream through lymphatic pathways (15, 16). Studies also indicated that lymphatic transport of nanoparticles (e.g., polypropylene sulfide) was size-dependent with more efficiency for smaller (25 nm) than larger (100 nm) particles (17). Skin penetration is also possible for some nanomaterials. Recent studies demonstrated that carboxylated quantum dots applied topically could penetrate the skin of SKH-1 mice (18), and PEG-coated quantum dots penetrated dermabraded mouse skin but not intact mouse skin (19). Recent studies have demonstrated that intact porcine skin is refractory to TiO_2 penetration (20), even with repeated administration over a 4 weeks period (21); however, neither of these studies were able to rule out the possible penetration of TiO_2 though damaged porcine skin and presentation to the dendritic or Langerhans cells of the skin.

The biological effects of TiO_2 nanoparticle exposure and the mechanisms behind the response are not well understood. Field studies found airborne anatase TiO_2 nanoparticles induced cytotoxicity response in human beings during the manufacturing process (22). Pulmonary toxicity of TiO_2 nanoparticles has been examined using mouse models (23-26), and the lung inflammatory and cytotoxicity response were likely related to the particle size (24, 26), but some studies suggested no such relationships (23). To elucidate the mechanisms involved in TiO_2 nanoparticle induced toxicity, a few studies have been reported. For example, *in vivo* studies indicated that TiO_2 nanoparticles bound tightly to DNA in the TiO_2 exposed mouse liver (27), could induce genotoxicity (28) and spleen injury (29). Exposure of lymphocytes to TiO_2 nanoparticles significantly increased micronucleus formation and DNA breakage, elevation of p53 level, activation of DNA damage checkpoint kinases, and generation of reactive oxygen species (ROS) (30). An *in vitro* study also suggested that TiO_2 nanoparticles could disrupt the function of proteins such as lysozyme activity inhibition (31) and Aβ fibrillation promotion by shortening the nucleation process (32). The interactions between nanoparticles and proteins (33-35) could be associated with nanoparticle size and surface properties. In addition, nonporous TiO_2 nanoparticles could slow the kinetics of chemical messenger secretion without altering the number of molecules released from the mast cell granules (36). The prospective response of immune system to TiO_2 nanoparticles are also under investigation (2, 37).

Omics techniques have been employed for the characterization of global molecular changes associated with nanoparticle exposure to biological systems. Microarray analysis of gene expression in zebrafish embryos exposed to TiO_2 nanoparticles demonstrated that different sizes of TiO_2 nanoparticles had varying effects on the expression of genes involved in the immune response, tumor necrosis factor, and endocytosis (38). Metabolomic analysis of urine samples from rats intragastrically administrated TiO_2 nanoparticles suggested that they could disturb energy and amino acid metabolisms and the gut microflora environment (39). Using 2-dimensional differential gel electrophoresis (2D-DIGE) and MALDI-MS, Yang *et al.* identified 16 differentially expressed proteins as a result of SiO_2 nanoparticle exposure to HaCaT cells (40). Nevertheless, characterization of *in vivo* biological effects of nanomaterials has not been fully explored and proteomic analysis of nanomaterial exposure is in its infancy. Information from global quantitative proteome analysis would enhance our understanding of nanomaterial-induced biological effects. In recent years, enzyme-catalyzed ^{18}O labeling (41) combined with multidimensional LC separation and tandem mass spectrometry (LC-MS/MS) has been successfully developed and applied to global quantitative proteome analysis(42). In this study, the technique was applied to the measurement of proteome changes in mouse lymph nodes upon intradermal injection of commercial TiO_2 nanoparticles. By comparing the lymph node proteomes of the TiO_2 nanoparticle-treated mice with that of the control group, we found interesting information related to the biological consequence of TiO_2 exposure to lymph nodes at the proteome level.

2. Materials and Methods

2.1. Chemicals and reagents

Ammonium bicarbonate (NH_4HCO_3), ammonium formate (NH_4HCO_2), Cremophor, guanidine hydrochloride (Gdn·HCl), iodoacetamide, and Tris were purchased from Sigma-Aldrich (St. Louis, MO). Formic acid and trifluoroacetic acid (TFA) were from Fluka (Milwaukee, WI). HPLC grade acetonitrile (CH_3CN) and water were obtained from Fisher Scientific (Fair Lawn, NJ). Tris(2-carboxyethyl)phosphine hydrochloride (TCEP·HCl), Excellulose desalting columns (5K MWCO) and Bicinchonic acid (BCA) protein assay reagent kit were purchased from Pierce (Rockford, IL). Chemicon total protein extraction buffer containing protease inhibitors cocktail was from Millipore (Billerica, MA). Ethyl alcohol was obtained from Pharmco-AAPER (Hopkinsville, KY).

2.2. TiO$_2$ nanoparticles

"Aeroxide" P25 TiO_2 (Baker and Collinson, Inc., Detroit, MI) nanoparticles were chosen for this study. Quantitative elemental analysis by ICP/AES for titanium indicated a purity of greater than 99%. X-Ray diffraction confirmed that the titanium dioxide consisted of a mixture of 86% anatase and 14% rutile phases. Transmission electron microscopy found the minimum particle size was 14.2 nm and the maximum particle size was 64.6 nm. The arithmetic mean was 27.5 ± 9.8 nm. The morphology of these particles was generally round, but they were irregular in shape (that is, some sharp edges were present and some particles were elongated). These results agreed well with the manufacturer's reported value of 21 nm. Surface area measurements (BET analysis) indicate that the internal surface area attributed to pores is between 2.2 and 3.3 m^2/g depending on whether the adsorption or desorption isotherm is used. The ideal surface area for smooth particles was calculated to be 50.5 m^2/g compared to an actual measured value of 50.9 ± 0.2 m^2/g by BET. This indicates that λ =1.01 or approximately 1% of the measured surface area is due to surface roughness. The determined BET value agreed with the manufacturer's reported value of 49 m^2/g.

2.3. Animal Treatment

Isolator reared, Helicobacter-free female Crl: SKH-1 (hr/hr) hairless mice were obtained from Charles River (Portage, MI) at 5 weeks of age. The mice were housed for 2 weeks in the National Center for Toxicological Research (Jefferson, AR) Quarantine Facility and acclimated for an additional week prior to use. The treatment of the mice was approved by the Institutional Animal Care and Use Committee at this American Association for Laboratory Animal Science accredited facility. At 9 weeks of age, groups of six mice were weighed (average body weight of 23 g) and anesthetized intraperitoneally with sodium pentobarbital (25 mg/kg body weight). Anesthetized mice were injected intradermally in both the left and right dorsal flanks with either 5 μl of 1:1:8 ethyl alcohol:cremophor:water vehicle or suspensions of nanoscale TiO_2 (1 mg/ml, DeGussa P25) in this vehicle using a Hamilton gas-tight syringe (Hamilton Company, Reno, NV) equipped with a 3/8-in., 26-gauge needle with a 30° (intradermal) bevel. The mice were euthanized using gaseous CO_2 24 hrs post injection and both the right and left brachial, axillary and inguinal lymph nodes were collected and immediately frozen in liquid nitrogen at necropsy.

2.4. Lymph node proteome extraction and trypsin digestion

The right brachial, axillary and inguinal lymph nodes from each mouse were combined and lysed. After adding 100 μL of Chemicon total protein extraction buffer, the lymph nodes were ground using a 1 mL Dounce tissue grinder (Wheaton Science International, Millville, NJ). The resulting lysates were centrifuged at $11,000 \times g$ for 20 min at 4 °C and the supernatants were collected. Protein concentrations were measured by the BCA protein assay. Equal amounts of protein from three TiO_2 nanoparticle treated mice were combined, as was the protein from the 3 control mice. The extracted proteome samples from both the treatment and control groups were desalted using Excellulose desalting columns and lyophilized. Protein samples were re-dissolved with 6 M Gdn·HCl in 50 mM Tris-HCl, pH 8.3. The samples were reduced by adding TCEP·HCl to the final concentration of 10 mM and boiling in a water bath for 10 min. Proteins were further alkylated in 50 mM iodoacetamide with an incubation at 37 °C in dark for 2 hrs. After alkylation, each sample was buffer-exchanged to 25 mM NH_4HCO_3 (pH 8.3) through an Excellulose desalting column (5K MWCO, Pierce, Rockford, IL) that was pre-equilibrated with 25 mM NH_4HCO_3 (pH 8.3). The samples were digested with trypsin (Promega, Madison, WI) at 37 °C for 16 hrs using a protein to enzyme ratio of 50:1 (w/w). The tryptic peptides were further cleaned by Alltech Extract-Clean SPE C18 HC column (Grace, Deerfield, IL). Samples were lyophilized and stored at -80 °C.

2.5. Trypsin-catalyzed $^{16}O/^{18}O$ labeling

Peptide C-terminal $^{16}O/^{18}O$ labeling was performed as described previously (43). For ^{18}O labeling, 50 μg of proteome tryptic peptides from the TiO_2 nanoparticle treated mouse group were dissolved in 17% CH_3CN in ^{18}O-enriched water (97%, Sigma-Aldrich, St. Louis, MO). Sequencing grade modified trypsin (Promega, Madison, WI) dissolved in ^{18}O-water was added to the samples at a ratio of 30:1 (w/w, protein-to-trypsin), and the mixture was incubated at 37 °C for 16 hrs. The reactions were quenched by boiling the samples for 10 min in a water bath and then cooling down to room temperature, followed by addition of 0.2% TFA. The sample was immediately lyophilized to dryness. The identical procedure was carried out in parallel for ^{16}O labeling of the same amounts of peptides from the control group in which the regular ^{16}O-water was used instead of ^{18}O-water. In addition, reverse labeling was performed as well in which the sample from TiO_2 nanoparticle treated mouse group was labeled using ^{16}O-water while the control sample was labeled using ^{18}O-water. The ^{16}O- and ^{18}O-labeled samples stored separately at -80 °C for further analysis.

2.6. Strong cation exchange liquid chromatographic (SCXLC) fractionation

Prior to SCXLC fractionation, each pair of ^{16}O-labeled and ^{18}O-labeled samples were dissolved in 25% CH3CN/0.1% TFA and combined (i.e., ^{16}O-control/^{18}O-treatment pair or ^{18}O-control/^{16}O-treatment pair). A Dionex UltiMate 3000 Nano and Cap LC system (Dionex Softron GmbH, Germering, Germany) was used to deliver mobile phase A (25% CH$_3$CN in water) and mobile phase B (25% CH$_3$CN/0.5 M NH$_4$HCO$_2$, pH 3.0). The ^{16}O/^{18}O-labeled peptides were loaded onto a 1 mm × 150 mm Polysulfoethyl A column (PolyLC Inc., Columbia, MD) and eluted at a flow rate of 50 μL/min, using the following NH$_4$HCO$_2$/CH$_3$CN multistep gradient: 3% mobile phase B for 5 min, followed a linear increase to 10% B for 18 min, a linear increase to 45% B for 26 min, then a linear increase to 100% B for 1 min, and maintained at 100% B for 10 min. The separation was monitored using a laser induced fluorescence detector equipped with 266 nm diode pumped solid state pulsed laser (ZETALIF Discovery, Picometrics, Toulouse, France) to detect native fluorescence at an emission wavelength of 340 nm. Thirty one fractions were collected at two-minute intervals. The fractions were lyophilized and stored at -80 °C for LC-MS/MS analysis

2.7. Nanoflow reversed-phase LC-MS/MS analysis

Nanoflow RPLC separation of peptides was conducted using a 9 cm long × 75 µm inner diameter (i.d.) fused silica capillary electrospray ionization (ESI) column which was coupled online to an Orbitrap mass spectrometer (LTQ-Orbitrap XL, Thermo Electron, San Jose, CA) for MS/MS analysis of each SCXLC fraction. The ESI column was slurry packed with 5 μm, 300 Å pore size Jupiter C18 RP particles (Phenomenex, Torrence, CA) against a 9 cm × 75 µm i.d. fused-silica capillary (Polymicro Technologies, Phoenix, AZ) with a flame-pulled fine i.d. (i.e., 5-7 μm) tip. Mobile phases A (0.1% formic acid in water) and B (0.1% formic acid in CH$_3$CN) were delivered by a Dionex UltiMate 3000 Nano and Cap LC system (Dionex Softron GmbH, Germering, Germany). Peptides were loaded in 30 min while the column was maintained with 2% solvent B at a flow rate of 1 µL/min, and then separated using a step gradient of 2%-42% solvent B for 65 min and 42%-98% solvent B for 15 min at a flow rate of ~250 nL/min. Following the MS survey scan with a resolution of 6×10^4 and a mass range of *m/z* 300-1800 in the Orbitrap analyzer, data-dependent MS/MS scans were acquired in the linear ion trap analyzer in which the 7 most intense peptide molecular ions in the MS scan were sequentially and dynamically selected for subsequent collision-induced dissociation (CID) using a normalized collision energy of 35%. Dynamic exclusion was enabled with duration of 1 min to prevent repeated acquisition of MS/MS spectra of the same peptide for which the MS/MS spectrum had been acquired in the previous scan. Electrospray voltage was set at 1.6 kV, and the voltage and temperature for the ion source capillary were 47 V and 160 °C, respectively

2.8. Peptide identification

The raw MS/MS data were searched using the SEQUEST cluster running under BioWorks (Rev. 3.3.1 SP1) (Thermo Electron, San Jose, CA) against a mouse IPI proteome database (version 3.78, containing 54,928 protein sequence entries) downloaded from the European Bioinformatics Institute (EBI) (http://www.ebi.ac.uk). Reversed protein sequences of all the protein entries were added to the same database for an estimation of false identification rate. Peptide mass tolerance of 10 ppm and fragment ion tolerance of 1 Da were set with tryptic specificity allowing two missed cleavages. SEQUEST criteria were Xcorr ≥ 1.7 for [M +H]$^{1+}$ ions, ≥ 2.5 for [M+2H]$^{2+}$ ions and ≥ 3.2 for [M+3H]$^{3+}$ ions, and $P \le 0.01$ for identification of fully tryptic peptides. A dynamic 4.0085 Da modification on the C-terminus was also set in a single search to identify both ^{18}O-labeled peptides and peptides with normal C-terminus. In addition, dynamic oxidation of Met by the addition of one oxygen (+15.9949 Da) and Cys carboxyamidomethylation (+57.0215 Da) were included. These

criteria were applied to filter the peptide identifications from both forward and reversed protein sequences.

2.9. Quantitation, normalization and statistical analysis

The identified peptides were quantified using the BioWorks' PepQuan module (Thermo Electron, San Jose, CA), which calculated the relative abundance (e.g., ratios of $^{18}O/^{16}O$, H/L) of peptides based on the areas of their extracted ion chromatograms (XIC) using a minimum intensity threshold of 100 counts, mass tolerance of 0.03 Da and smoothing point of 5. After logarithmic transformation, the abundance ratio distribution of all the peptides in each dataset was plotted to fit with normal distribution and nonlinear regression was performed according to the method described previously (44). The mean ratio was used to normalize the abundance ratios of the dataset. When multiple peptides were identified from the same protein, an average ratio was calculated. Student's t-test was performed for the proteins in each quantitative dataset and *p* value was calculated.

2.10. Pathway and network analysis

To investigate the pathways and networks involving the lymph node proteins differentially expressed between the control and TiO_2 nanoparticle treated mice, the MetaCore (GeneGo, St. Joseph, MI) program was used to build protein interaction networks. MetaCore is an integrated software suite for functional analysis of experimental data and it contains curated protein interaction networks on the basis of manually curated database of human, mouse, rat protein-protein, protein-DNA, protein-RNA and protein-compound interactions. The significantly changed proteins from our experiments and the proteins from the MetaCore database were used to generate networks using the shortest paths algorithm (maximum 2 steps in the path) and pre-filters as lymphocyte and mouse (*M. musculus*).

3. Results

3.1. Forward and reverse trypsin-catalyzed $^{16}O/^{18}O$ labeling strategy for confident quantitation

Enzyme-catalyzed oxygen exchange has been used for stable isotope labeling in quantitative proteomics. The labeling is performed typically by incubation of peptides with trypsin in the presence of ^{18}O-coded water (45). The two oxygen atoms in the C-terminal carboxylate group of a peptide are exchanged with two ^{18}O atoms from the water, resulting in an addition of 4.0085 Da to the peptide. This labeling technique has been applied to many quantitative proteomic studies for relative quantitation of protein expression. However, oxygen back-exchange during sample processing and analysis and/or incomplete labeling especially for proteome samples have been reported (46). The labeling technique has been improved to achieve complete labeling and prevent oxygen back-exchange (42, 47, 48). These improvements include decoupling of ^{18}O labeling from the protein digestion step (42, 47), ^{18}O labeling performed in a buffer containing 20% methanol which enhances trypsin activity (42), and inhibition of post-labeling trypsin activity by thermal deactivation to prevent oxygen back-exchange in ^{18}O-labeled samples (47, 48). To overcome the described potential issues and eliminate protein quantitation errors, we carried out both forward and reverse $^{16}O/^{18}O$ labeling in parallel for the same pair of control and TiO_2 nanoparticle treated mouse lymph node proteomes. The quantitative proteomic approach employing this labeling strategy is illustrated in Figure 1. The protein samples of lymph nodes from the control and TiO_2 nanoparticle treated mice were firstly digested with trypsin and desalted. Fifty micrograms of peptides from the TiO_2 nanoparticle treated mouse lymph nodes were labeled with ^{18}O and mixed in equal amounts with ^{16}O-labeled control sample to form the forward labeling mixture as defined here. In reverse labeling, the control sample was ^{18}O-labeled while the treated sample was ^{16}O-labeled. The resulting two mixtures were

individually separated using SCX liquid chromatography into 31 fractions, and each SCX fraction was analyzed by nanoflow RPLC-MS/MS.

Careful examination of MS data from both forward and reverse labeled samples suggest that ^{18}O labeling for a vast majority of peptides was generally complete and no obvious oxygen back-exchange was observed during the experiment. Although a systematic evaluation has not been done on the factors that might contribute to oxygen back-exchange, the samples were handled in a way to minimize if not eliminate this problem. Even when samples were kept at 5 °C for 2 days in the HPLC sample tray, there was no obvious oxygen back-exchange observed (data not shown). An example illustrating ^{18}O labeling efficiencies in both forward and reverse approaches is shown in Figure 2. Three and four pairs of relatively abundant MS peaks with LC elution time of approximately 25 min and 38 min, respectively, were detected in the defined mass ranges from a fraction of forward ^{18}O-labeled sample as shown in Figure 2A and 2B. The corresponding peaks of the same peptides from the reverse labeling are shown in Figure 2C and 2D, respectively. For these peptide pairs, the abundance ratios of $^{16}O/^{18}O$ are generally 1:1, showing no significant changes in expression. A careful comparison of the ^{18}O-labeled (heavy) peptides (the TiO$_2$ nanoparticle treatment) at m/z 754.3986, 790.4017 and 817.8959 with their ^{16}O-countparts (light, the control) reveals that these ^{18}O-peptides are 8.4%, 15.5% and 15.7% higher in abundance, respectively (Figure 2A). In the reverse labeling, the same peptides from the TiO$_2$ nanoparticle treated sample are ^{16}O-labeled. As shown in Figure 2C, the ^{16}O-labeled peptides at m/z 752.3961, 788.3993 and 815.8936 are 7.2%, 18.3%, 6.6% more abundant than the ^{18}O-countparts. Similar results are observed for the peaks in Figure 2B and 2D.

To examine the overall efficiency of forward and reverse ^{18}O labeling and compare the quantitation variance at the whole proteome level, statistical distribution was plotted for the 7030 common unique peptides (Figure 4) identified and quantified from both forward and reverse ^{18}O labeling experiments. A normal distribution was obtained in terms of the number of unique peptides plotted within binned *log$_2$ ratio* for both labeling approaches (Figure 3A). These distributions were quite similar, indicating ^{18}O labeling was highly reproducible. Nonlinear regression analyses indicated that both datasets had similar coefficients of determination (R^2=0.9823 for forward labeling, and R^2=0.9856 for reverse labeling). The standard deviation (σ) of the two datasets was close as well with the values of 0.2676 for forward labeling and 0.2761 for reverse labeling. The standard deviation values were back-calculated to an approximate ratio of 1.2 for both labeling approaches. It should be noted that the real abundance change in the peptide ratio datasets were implied in the calculated abundance ratio, the actual standard deviation owing to incomplete ^{18}O labeling would be less. The above analyses indicate that a vast majority of the peptides have a ratio of or close to 1:1, as illustrated in Figure 3A as well. The results from this study are similar to or better than some previously published large-scale ^{18}O labeling datasets (49).

Since forward and reverse ^{18}O labeling approaches were employed in this study, another way to evaluate the overall labeling efficiency is to calculate the quantitation variance between forward and reverse labeling analyses for the same peptides. Theoretically, the coefficient of variation (CV, %) of the abundance ratios of the same peptide from forward and reverse ^{18}O labeling should be zero if the labeling is complete, i.e., the peptide has exactly the same ratio. Calculation of CV for the 7030 common unique peptides (Figure 4) quantified from both forward and reverse ^{18}O labeling experiments revealed that approximately 37%, 22%, and 13% of the peptides had CVs of <10%, 10-20%, and 20-30%, respectively (Figure 3B). Therefore, a total of 72% of the peptides had CV values less than 30%. Nonetheless, it should be pointed out that the actual number could be more than 72% since the ratio variance between forward and reverse labeling was originated not only from incomplete labeling but also from other factors such as errors in peptide peak integration,

etc. Taken together, these data suggest that the overall ^{18}O labeling efficiency in this study is high at the proteome level and consistent quantitation can be achieved between forward and reverse ^{18}O labeling. For a limited number of peptides with incomplete labeling, the abundance ratios of the same peptide from forward and reverse labeling are inconsistent. By comparing the quantitative data from forward and reverse labeling approaches, quantitation error resulted from incomplete labeling can be eliminated, thus confident results can be obtained.

3.2. Quantitative proteomic analysis of mouse lymph nodes upon DeGussa P25 TiO$_2$ nanoparticle treatment

To identify protein expression alterations in mouse lymph nodes associated with DeGussa P25 TiO$_2$ nanoparticle treatment, both forward and reverse trypsin-catalyzed ^{18}O-labelings were employed as described previously to achieve reliable and confident protein quantitation. A total of 25,069 and 23,144 peptides, corresponding to 9,332 and 9,345 unique peptide sequences regardless of ^{16}O/^{18}O labeling, were identified and quantified from forward and reverse labeling experiments respectively using the Xcorr criteria defined in the methods and $p{\leq}0.01$ (Figure 4). The false discovery rate (FDR) was estimated to be <0.1% at the peptide level for these peptide datasets as a result of a reversed protein sequence database search. Approximately 75% of these unique peptides overlapped between forward and reverse labeling experiments. From these indentified peptides, a total of 2,809 and 2,818 proteins were identified and quantified from the forward and reverse labeling, respectively, with 2,390 proteins identified commonly (i.e., ~85% overlap) from these two labeling approaches (Figure 4).

An evaluation of quantitation errors and statistic analysis was performed for the identification of reliable protein expression changes as a result of TiO$_2$ nanoparticle treatment. The CV (%) of the abundance ratio was calculated for each protein with multiple identifications. The average CV of all the proteins with multiple IDs within each of the two labeling experiments was approximately 30%. In addition, Student's t-test was performed for each protein with multiple peptide identifications to examine whether the protein abundance change as a result of TiO$_2$ nanoparticle treatment was statistically significant or not as compared to the control. By using $p<0.05$ from this t-test, proteins with single peptide identifications or with high quantitative standard deviation were excluded from further consideration. Based on the CV data and application of the t-test, we set 1.3-fold protein abundance changes (the abundance ratio of treatment to control was ≥ 1.3 or ≤ 0.77) with statistical significance $p<0.05$ to define differentially expressed proteins, which must also be consistently observed from both forward and reverse labeling experiments. As a result, 19 lymph node proteins were up-regulated and 14 were down-regulated in the mice treated with TiO$_2$ nanoparticles compared to control animals. The quantitative data along with subcellular localization of these significantly changed proteins are summarized in Table 1. The detailed peptide identification information such as individual peptide fold change, Xcorr, DeltaCn and so forth were listed in Supplementary Table 1.

For the peptides from the 33 differentially expressed proteins, almost half of them (49%) are methionine (Met)-containing peptides or the peptides with missed cleavage sites. Jorge *et al.* discussed that peptides containing missed cleavage sites or oxidized Met residues do not reliably reflect correct protein concentrations (49); however, Bonzon-Kulichenko *et al.* argued that partial digestions and Met oxidation do not affect protein quantification and that variances at the scan, peptide, and protein levels are stable and reproducible(50). The results from this experiment are in agreement with Bonzon-Kulichenko's observation in that a vast majority of the peptides containing Met residues or from partial digestion had consistent fold changes between the forward and reverse ^{18}O labeling experiments and the abundance changes of these peptides were in agreement with other regular peptides within the same

protein. Approximately 4% of Met-containing or partially digested peptides had inconsistent fold changes between the forward and reverse ^{18}O labeling analyses. The results from this study along with those from other laboratories suggest that quantification reliability of Met-containing or partially digested peptides depends on the experimental procedures and conditions used for sample preparation.

Among the differentially expressed proteins, most of them are cytoplasmic and nuclear proteins while there are only three secreted and two plasma membrane proteins. Biological function annotation indicates that most altered proteins are involved in immune response (e.g., inflammation) and antimicrobial activity, lipid and fatty acid metabolism, mRNA processing, and nucleosome assembly. Proteins associated with immune response and antimicrobial activity include protein S100-A8, S100-A9, chitinase-3-like protein 3, amine oxidase, cathelin-related antimicrobial peptide, and lactotransferrin. These proteins were down-regulated upon TiO$_2$ nanoparticle treatment except for amine oxidase. Another class of down-regulated proteins are related to mRNA processing (e.g., splicing), encompassing cleavage and polyadenylation specificity factor subunit 6 (CPSF6), Luc7-like protein 3, proline- and glutamine-rich splicing factor, serine/arginine-rich splicing factors 2 and 3, splicing factor U2AF 65 kDa subunit, and probable ATP-dependent RNA helicase DDX46. As an example, Figure 5A shows an MS/MS spectrum of the ^{18}O-labeled peptide DYM*DTLPPTVGDDVGK from protein CPSF6. The MS spectra of ^{16}O/^{18}O-labled peptide pairs indicate that the abundance ratios are consistent between the forward (^{18}O/^{16}O=0.63) and reverse (^{16}O/^{18}O=0.70) labeling (Figure 5B), suggesting protein CPSF6 was down-regulated in the mouse lymph nodes due to DeGussa P25 TiO$_2$ nanoparticle treatment. In contrast, proteins associated with lipid and fatty acid metabolism were up-regulated, which include perilipin-1, monoglyceride lipase, enoyl-CoA hydratase, medium-chain specific acyl-CoA dehydrogenase, ATP-citrate synthase, acetyl-Coenzyme A carboxylase beta, pyruvate carboxylase, and adipocyte fatty acid-binding protein. Four of them are mitochondrial proteins. In addition, histone H1, H2A, H2B and H4, which are responsible for nucleosome assembly, were up-regulated.

3.3. Pathway and network analysis of differentially expressed proteins

The 33 differentially expressed proteins (Table 1) were subjected to molecular network analysis by MetaCore program (GeneGo, Inc, St Joseph, MI) using the shortest paths algorithm (maximum 2 steps in the path for interaction) and pre-filters as lymphocyte and *M musculus*. Figure 6 shows the most significant network resolved, which includes 15 differentially expressed proteins and the 10 proteins in the MetaCore database. One of the main hubs in the network is the ESR1 (estrogen receptor) whose transcriptional activity is regulated by multiple signaling pathways (thick cyan lines) (51). Lactoferrin is the only differentially expressed protein interacting directly with ESR1. Another hub is c-Myc, which directly interacts with 5 differentially expressed proteins (ACADM, HMGB1, IP-30, PSF, and PYC). Interestingly, PPARγ is a hub that mainly connects up-regulated proteins (A-FABP, Perilipin, and PYC) involved in lipid metabolism except for SFRS3. It has been reported that U2AF-65 physically interacts with CPSF6 and increases its activity (52). Our results indicated that both U2AF-65 and CPSF6 were down-regulated after TiO$_2$ nanoparticle treatment. It is also worth noting that calgranulin A and B interact with each other and increase their activities in normal circumstances (53), but this study showed that they were down-regulated. An analysis of this network revealed that the top five biological processes involved by those differentially expressed proteins are cellular responses to stimulus, stress, organic substance, multi-organism process and chemical stimulus (Table 2).

4. Discussion

In this study, 2390 proteins were commonly identified and quantified from forward and reverse trypsin-catalyzed $^{16}O/^{18}O$ labelings of the proteins extracted from the control and TiO_2 nanoparticle-treated mouse lymph nodes, using combined SCX fractionation and nanoflow LC-MS/MS experiments. Compared to early studies employing two-dimensional gel electrophoresis (2-DE) combined with mass spectrometry (54-58), protein coverage for mouse lymph nodes was significantly increased in this study.

The TiO_2 nanoparticle employed here is DeGussa P25. The average particle size is ~28 nm and the specific surface area is ~51 m^2/g. Early studies showed that nanoparticles traffic to the draining lymph nodes in a size-dependent manner, where micron-sized particles required dendritic cells to transport them from the injection site to lymph nodes. In contrast, small nanoparticles (20-200 nm) and virus-like particles (30 nm) were transported to lymph nodes through free drainage, and it would take two or more hours for nanoparticles of 30 nm or less to travel to lymph nodes (59). The migrated nanoparticles could remain in the lymph nodes for days. A recent study of organic nanoparticles and inorganic/organic hybrid nanoparticles also reported the rapid transportation of nanoparticles with hydrodynamic diameter (HD) less than 34 nm and a noncationic surface charge from the lung to mediastinal lymph nodes (60). In order to determine the impact of the TiO_2 nanoparticles on the lymph node proteome, we selected the 24 hr time-point to allow sufficient time for them to be to present in the lymph nodes.

In previous *in vivo* studies using a high dose of TiO_2 nanoparticles, liver DNA cleavage (27), genotoxicity (28) and spleen injury (29) were found. Trouiller *et al.* (28) discovered DeGussa P25 TiO_2 nanoparticles induced 8-hydroxy-2′-deoxyguanosine, gamma-H2AX foci, micronuclei, and DNA deletions after treating mice daily with in their drinking water containing DeGussa P25 TiO_2 nanoparticles up to 0.6 mg/mL for 5 days (100 mg/kg body weight daily). Li *et al.* (27) found intraperitoneal injection of anatase TiO_2 nanoparticles (~5 nm) at a daily dose of 150 mg/kg body weight for 14 days could cause liver DNA cleavage and hepatocyte apoptosis in mice. Li *et al.* (29) also found spleen injuries after the same high dose treatment of mice for 45 days. In comparison, our study introduced DeGussa P25 TiO_2 nanoparticles into mice at a low dose (~0.2 mg/kg body weight) through intradermal injection and their effects were evaluated after 24 hours. The low dose TiO_2 nanoparticle treatment allows the early assessment of protein expression changes in the mouse lymph nodes exposed to TiO_2 nanoparticles before the apparent pathological damages are observed. Results from this study indicate this treatment affected only 33 proteins (up- or down-regulated using a filter of ≥1.3 fold and $p<0.05$), which occupied only ~1% of the total number of proteins quantified. This subset of proteins could represent early response proteins to the perturbation with exogenous TiO_2 nanoparticles.

A set of proteins associated with the immune response and antimicrobial activity were down-regulated (i.e., CAMP, LTF, S00A8, S00A9, and CHI3L3) except for amine oxidase (AOC3) which was up-regulated as a result of TiO_2 nanoparticle treatment. Network analysis indicated that ESR1 interacts with lactotransferrin (LTF) (Figure 6), an important iron-binding protein that declined about three folds. Lactotransferrin (i.e., lactoferrin) is present in milk and other body secretary fluids with an antimicrobial activity. In the non-specific immune system, lactoferrin performs multiple functions such as iron homeostasis regulation, host defense against microbial infections, anti-inflammation activity, regulation of cellular growth and differentiation, and protection against cancer development and metastasis. Studies have suggested that nuclear hormone receptor ESR1 can bind the *LTF* promoter and activate its expression (51). However ESR1 was not identified directly in this experiment. Related proteins in the identified network are calgranulin A (S100A8) and B

(S100A9). Both proteins participate in the inflammatory amphoterin signaling network. Calgranulin A and B proteins are two Ca^{2+}-binding proteins of the S100 family. The two proteins can form a heterodimer and leukocyte L1 antigen complex, present in the serum and interstitial fluid in several infectious and/or inflammatory disorders, and may play an important role in leukocyte trafficking (53). Calgranulin A/B dimer was reported to be membrane-associated and present in acute inflammation but absent in chronic inflammation (61). Down-regulation of calgranulin A and B and other immune responsive proteins after TiO_2 nanoparticle treatment may suggest potential early signs of low level/chronic inflammation or the immediate immune response of lymph nodes at the molecular level as a result of low dose treatment.

A class of lipid and fatty acid metabolism-related proteins was up-regulated as described early. Protein network analysis indicated that PPARγ is one of the major hubs in the significantly altered network. PPARγ protein, albeit not identified and quantified, is a regulator of adipocyte differentiation. The genes activated by PPARγ stimulate lipid uptake and adipogenesis by adipocytes (62). In the identified network (Figure 6), downstream proteins of PPARγ include lipid droplet-associated protein perilipin-1, adipocyte-type fatty acid-binding protein (A-FABP) and pyruvate carboxylase (PYC). These proteins are associated with lipid/fatty acid metabolism and were all up-regulated upon TiO_2 nanoparticle treatment. PPARγ also interacts with serine/arginine-rich splicing factor 3 (SFRS3) gene promoter but the binding effect was not clear (63). However, SFRS3 is associated with c-Myc as well. It may be related to mRNA processing. In our study, SFRS3 was down-regulated upon TiO_2 nanoparticles treatment. Up-regulated lipid metabolism proteins that are directly or indirectly associated with c-Myc include PYC, medium-chain specific acyl-CoA dehydrogenase (ACADM) and ATP-citrate synthase (ACLY). Currently, it is not clear what effects of up-regulation of lipid metabolism proteins are on the functions of mouse lymph nodes, and further studies are needed.

TiO_2 nanoparticle treatment also resulted in expression changes of other groups of proteins such as mRNA processing proteins and histone isoforms. Seven proteins associated with mRNA processing/splicing (i.e., CPSF6, DDX46, SFPQ, SRSF2, SRSF3, and U2AF-65) were down-regulated in TiO_2 nanoparticle-treated mice. There are more than one hundred fifty proteins involved in mRNA processing. Down-regulation of seven of them may not suggest the slowdown of mRNA processing. Likewise, transcription factor c-Myc is believed to regulate the expression of ~15% of all the genes including those involved in cell division, cell growth, and apoptosis (64). In this study, however, only a few proteins whose abundance changed because of treatment were identified to be regulated by c-Myc and these proteins are mainly related to mRNA processing or lipid metabolism although c-Myc is one of the major hubs in the significantly altered protein network. Interestingly, histone isoforms H1, H2A, H2B and H4 were up-regulated upon TiO_2 nanoparticle treatment. However, histone H3 was identified with only one unique peptide from the forward ^{18}O-labeled sample, and the abundance change was less than 1.3-fold. Since the TiO_2 nanoparticle treatment was in low doses and analysis was conducted at an early time point, the differentially expressed proteins identified in the current experiment could represent early response proteins to this type of perturbation. With extended treatment with a low dose of this nanoparticle, further protein alterations could be observed or, conversely, the lymph nodes might adapt. When high doses of TiO_2 nanoparticles are employed for relative long time (days to weeks) treatment, more proteins might be expected to be changed in expression and be more apparently associated with pathological changes as observed in the previous studies (27-29).

5. Conclusions

Alterations in protein expression levels in mouse lymph nodes in response to low dose and short treatment time with DeGussa P25 TiO_2 nanoparticles were analyzed using trypsin-catalyzed $^{16}O/^{18}O$ labeling in conjunction with two-dimensional LC separation and tandem mass spectrometry. Forward and reverse $^{16}O/^{18}O$ labeling resulted in quantification of 2809 and 2818 proteins, respectively, with a total of 2390 proteins commonly quantified from both labeling approaches. While ^{18}O labeling was generally complete, more confident quantification could be achieved by comparing the consistency of protein abundance ratios of forward and reverse $^{16}O/^{18}O$ labeling. A total of 19 lymph node proteins were up-regulated and 14 were down-regulated over 1.3 fold with $p<0.05$, in the mice treated with TiO_2 nanoparticles. This accounted for approximately 1% (33 proteins) of the total proteins identified from mouse lymph nodes. Biological function annotation indicates that the abundance changed proteins mainly involve in immune response (e.g., inflammation) and antimicrobial activity, lipid and fatty acid metabolism, mRNA processing, and nucleosome assembly. Protein network analysis indicates that the main regulators of protein expression could be estrogen receptor (ESR1), PPARγ, and c-Myc signalings. The differentially expressed proteins identified in this experiment could represent early response proteins to TiO_2 nanoparticle treatment in mouse lymph nodes although their functions need to be further explored in relation to this type of perturbation.

Supplementary Material

Refer to Web version on PubMed Central for supplementary material.

Acknowledgments

References

1. Schultz, WB.; Barclay, L. A hard pill to swallow: Barriers to effective FDA regulation of nanotechnology-based dietary supplements. Woodrow Wilson International Center for Scholars; Washington, DC: 2009. p. 1-28.

2. Dobrovolskaia MA, McNeil SE. Immunological properties of engineered nanomaterials. Nat Nanotechnol. 2007; 2:469–478. [PubMed: 18654343]

3. Lammers T, Hennink WE, Storm G. Tumour-targeted nanomedicines: principles and practice. Br J Cancer. 2008; 99:392–397. [PubMed: 18648371]

4. Handy RD, Shaw BJ. Toxic effects of nanoparticles and nanomaterials: implications for public health, risk assessment and the public perception of nanotechnology. Health Risk Soc. 2007; 9:125–144.

5. Maynard AD, Aitken RJ, Butz T, Colvin V, Donaldson K, Oberdorster G, Philbert MA, Ryan J, Seaton A, Stone V, Tinkle SS, Tran L, Walker NJ, Warheit DB. Safe handling of nanotechnology. Nature. 2006; 444:267–269. [PubMed: 17108940]

6. Sundaram SK, Weber TJ. Special issue: on nanotoxicity. Int J Nanotechnol. 2008; 5:1–2.

7. Sweet L, Strohm B. Nanotechnology - life-cycle risk management. Hum Ecol Risk Assess. 2006; 12:528–551.

8. Landsiedel R, Ma-Hock L, Kroll A, Hahn D, Schnekenburger J, Wiench K, Wohlleben W. Testing metal-oxide nanomaterials for human safety. Adv Mater. 2010; 22:2601–2627. [PubMed: 20512811]

9. Xu LG, Liu Y, Bai R, Chen CY. Applications and toxicological issues surrounding nanotechnology in the food industry. Pure Appl Chem. 2010; 82:349–372.

10. Fischer HC, Chan WC. Nanotoxicity: the growing need for in vivo study. Curr Opin Biotech. 2007; 18:565–571. [PubMed: 18160274]

11. Oberdorster G, Oberdorster E, Oberdorster J. Nanotoxicology: an emerging discipline evolving from studies of ultrafine particles. Environ Health Persp. 2005; 113:823–839.

12. Holgate ST. Exposure, uptake, distribution and toxicity of nanomaterials in humans. J Biomed Nanotechnol. 2010; 6:1–19. [PubMed: 20499827]

13. Sugibayashi K, Todo H, Kimura E. Safety evaluation of titanium dioxide nanoparticles by their absorption and elimination profiles. J Toxicol Sci. 2008; 33:293–298. [PubMed: 18670160]

14. Fabian E, Landsiedel R, Ma-Hock L, Wiench K, Wohlleben W, van Ravenzwaay B. Tissue distribution and toxicity of intravenously administered titanium dioxide nanoparticles in rats. Arch Toxicol. 2008; 82:151–157. [PubMed: 18000654]

15. Kim S, Lim YT, Soltesz EG, De Grand AM, Lee J, Nakayama A, Parker JA, Mihaljevic T, Laurence RG, Dor DM, Cohn LH, Bawendi MG, Frangioni JV. Near-infrared fluorescent type II quantum dots for sentinel lymph node mapping. Nat Biotechnol. 2004; 22:93–97. [PubMed: 14661026]

16. Gopee NV, Roberts DW, Webb P, Cozart CR, Siitonen PH, Warbritton AR, Yu WW, Colvin VL, Walker NJ, Howard PC. Migration of intradermally injected quantum dots to sentinel organs in mice. Toxicol Sci. 2007; 98:249–257. [PubMed: 17404394]

17. Reddy ST, van der Vlies AJ, Simeoni E, Angeli V, Randolph GJ, O'Neil CP, Lee LK, Swartz MA, Hubbell JA. Exploiting lymphatic transport and complement activation in nanoparticle vaccines. Nat Biotechnol. 2007; 25:1159–1164. [PubMed: 17873867]

18. Mortensen LJ, Oberdorster G, Pentland AP, DeLouise LA. In vivo skin penetration of quantum dot nanoparticles in the murine model: The effect of UVR. Nano Lett. 2008; 8:2779–2787. [PubMed: 18687009]

19. Gopee NV, Roberts DW, Webb P, Cozart CR, Siitonen PH, Latendresse JR, Warbitton AR, Yu WW, Colvin VL, Walker NJ, Howard PC. Quantitative Determination of Skin Penetration of PEG-Coated CdSe Quantum Dots in Dermabraded but not Intact SKH-1 Hairless Mouse Skin. Toxicol Sci. 2009; 111:37–48. [PubMed: 19574408]

20. Gontier E, Ynsa MD, Biro T, Hunyadi J, Kiss B, Gaspar K, Pinheiro T, Silva JN, Filipe P, Stachura J, Dabros W, Reinert T, Butz T, Moretto P, Surleve-Bazeille JE. Is there penetration of titania nanoparticles in sunscreens through skin? A comparative electron and ion microscopy study. Nanotoxicology. 2008; 2:218–231.

21. Sadrieh N, Wokovich AM, Gopee NV, Zheng JW, Haines D, Parmiter D, Siitonen PH, Cozart CR, Patri AK, McNeil SE, Howard PC, Doub WH, Buhse LF. Lack of significant dermal penetration of titanium dioxide from sunscreen formulations containing nano- and submicron-size TiO_2 particles. Toxicol Sci. 2010; 115:156–166. [PubMed: 20156837]

22. Liao CM, Chiang YH, Chio CP. Assessing the airborne titanium dioxide nanoparticle-related exposure hazard at workplace. J Hazard Mater. 2009; 162:57–65. [PubMed: 18554790]

23. Warheit DB, Webb TR, Sayes CM, Colvin VL, Reed KL. Pulmonary instillation studies with nanoscale TiO_2 rods and dots in rats: toxicity is not dependent upon particle size and surface area. Toxicol Sci. 2006; 91:227–236. [PubMed: 16495353]

24. Warheit DB, Webb TR, Reed KL, Frerichs S, Sayes CM. Pulmonary toxicity study in rats with three forms of ultrafine-TiO_2 particles: differential responses related to surface properties. Toxicology. 2007; 230:90–104. [PubMed: 17196727]

25. Lee K, Yang YS, Kwon SJ, Lee JS, Choi SJ, Seo HS, Kang MS, Lee BC, Kim SN, Yang HS, Han YA, Ryu HJ, Heo JD, Cho KH, Song CW. Lung injury study by 15 days inhalation exposure of titanium dioxide nanoparticles in rats. Toxicol Lett. 2009; 189:S186–S186.

26. Grassian VH, Adamcakova-Dodd A, Pettibone JM, O'Shaughnessy PT, Thorne PS. Inflammatory response of mice to manufactured titanium dioxide nanoparticles: Comparison of size effects through different exposure routes. Nanotoxicology. 2007; 1:211–226.

27. Li N, Ma LL, Wang J, Zheng L, Liu J, Duan YM, Liu HT, Zhao XY, Wang SS, Wang H, Hong FS, Xie YN. Interaction between nano-anatase TiO_2 and liver DNA from mice *in vivo*. Nanoscale Res Lett. 2010; 5:108–115. [PubMed: 20652136]

28. Trouiller B, Reliene R, Westbrook A, Solaimani P, Schiestl RH. Titanium dioxide nanoparticles induce DNA damage and genetic instability in vivo in mice. Cancer Res. 2009; 69:8784–8789. [PubMed: 19887611]

29. Li N, Duan YM, Hong MM, Zheng L, Fei M, Zhao XY, Wang J, Cui YL, Liu HT, Cai JW, Gong SJ, Wang H, Hong FS. Spleen injury and apoptotic pathway in mice caused by titanium dioxide nanoparticules. Toxicol Lett. 2010; 195:161–168. [PubMed: 20381595]

30. Kang SJ, Kim BM, Lee YJ, Chung HW. Titanium dioxide nanoparticles trigger p53-mediated damage response in peripheral blood lymphocytes. Environ Mol Mutagen. 2008; 49:399–405. [PubMed: 18418868]

31. Xu Z, Liu XW, Ma YS, Gao HW. Interaction of nano-TiO_2 with lysozyme: insights into the enzyme toxicity of nanosized particles. Environ Sci Pollut Res. 2010; 17:798–806.

32. Wu WH, Sun X, Yu YP, Hu J, Zhao L, Liu Q, Zhao YF, Li YM. TiO_2 nanoparticles promote beta-amyloid fibrillation *in vitro*. Biochem Biophys Res Commun. 2008; 373:315–318. [PubMed: 18571499]

33. Lundqvist M, Stigler J, Elia G, Lynch I, Cedervall T, Dawson KA. Nanoparticle size and surface properties determine the protein corona with possible implications for biological impacts. Proc Natl Acad Sci USA. 2008; 105:14265–14270. [PubMed: 18809927]

34. Gessner A, Waicz R, Lieske A, Paulke B, Mader K, Muller RH. Nanoparticles with decreasing surface hydrophobicities: influence on plasma protein adsorption. Int J Pharm. 2000; 196:245–249. [PubMed: 10699728]

35. Asuri P, Bale SS, Karajanagi SS, Kane RS. The protein-nanomaterial interface. Curr Opin Biotechnol. 2006; 17:562–568. [PubMed: 17015011]

36. Maurer-Jones MA, Lin YS, Haynes CL. Functional assessment of metal oxide nanoparticle toxicity in immune cells. ACS Nano. 2010; 4:3363–3373. [PubMed: 20481555]

37. Izhaky D, Pecht I. What else can the immune system recognize? Proc Natl Acad Sci USA. 1998; 95:11509–11510. [PubMed: 9751695]

38. Yeo MK, Kim HE. Gene expression in zebrafish embryos following exposure to TiO_2 nanoparticles. Mol Cell Toxicol. 2010; 6:97–104.

39. Bu Q, Yan GY, Deng PC, Peng F, Lin HJ, Xu YZ, Cao ZX, Zhou T, Xue AQ, Wang YL, Cen XB, Zhao YL. NMR-based metabonomic study of the sub-acute toxicity of titanium dioxide nanoparticles in rats after oral administration. Nanotechnology. 2010; 21

40. Yang XF, Liu JJ, He HW, Zhou L, Gong CM, Wang XM, Yang LQ, Yuan JH, Huang HY, He LH, Zhang B, Zhuang ZX. SiO_2 nanoparticles induce cytotoxicity and protein expression alteration in HaCaT cells. Part Fibre Toxicol. 2010; 7

41. Schnolzer M, Jedrzejewski P, Lehmann WD. Protease-catalyzed incorporation of O-18 into peptide fragments and its application for protein sequencing by electrospray and matrix-assisted laser desorption/ionization mass spectrometry. Electrophoresis. 1996; 17:945–953. [PubMed: 8783021]

42. Blonder J, Hale ML, Chan KC, Yu LR, Lucas DA, Conrads TP, Zhou M, Popoff MR, Issaq HJ, Stiles BG, Veenstra TD. Quantitative profiling of the detergent-resistant membrane proteome of Iota-b toxin induced Vero cells. Journal of Proteome Research. 2005; 4:523–531. [PubMed: 15822930]

43. Yu LR, Zhu ZY, Chan KC, Issaq HJ, Dimitrov DS, Veenstra TD. Improved titanium dioxide enrichment of phosphopeptides from HeLa cells and high confident phosphopeptide identification by cross-validation of MS/MS and MS/MS/MS spectra. J Proteome Res. 2007; 6:4150–4162. [PubMed: 17924679]

44. Yu LR, Chan KC, Tahara H, Lucas DA, Chatterjee K, Issaq HJ, Veenstra TD. Quantitative proteomic analysis of human breast epithelial cells with differential telomere length. Biochemical and Biophysical Research Communications. 2007; 356:942–947. [PubMed: 17395154]

45. Fenselau C, Yao XD. O-18(2)-Labeling in Quantitative Proteomic Strategies: A Status Report. Journal of Proteome Research. 2009; 8:2140–2143. [PubMed: 19338309]

46. Stewart II, Thomson T, Figeys D. O-18 labeling: A tool for proteomics. Rapid Commun Mass Sp. 2001; 15:2456–2465.

47. Storms HF, van der Heijden R, Tjaden UR, van der Greef J. Considerations for proteolytic labeling-optimization of O-18 incorporation and prohibition of back-exchange. Rapid Commun Mass Sp. 2006; 20:3491–3497.

48. Petritis BO, Qian WJ, Camp DG, Smith RD. A simple procedure for effective quenching of trypsin activity and prevention of O-18-labeling back-exchange. J Proteome Res. 2009; 8:2157–2163. [PubMed: 19222237]

49. Jorge I, Navarro P, Martinez-Acedo P, Nunez E, Serrano H, Alfranca A, Redondo JM, Vazquez J. Statistical model to analyze quantitative proteomics data obtained by ^{18}O/^{16}O labeling and linear Ion trap mass spectrometry: application to the study of vascular endothelial growth factor-induced angiogenesis in endothelial cells. Mol Cell Proteomics. 2009; 8:1130–1149. [PubMed: 19181660]

50. Bonzon-Kulichenko E, Perez-Hernandez D, Nunez E, Martinez-Acedo P, Navarro P, Trevisan-Herraz M, Ramos MD, Sierra S, Martinez-Martinez S, Ruiz-Meana M, Miro-Casas E, Garcia-Durado D, Redondo JM, Burgos JS, Vazquez J. A robust method for quantitative high-throughput analysis of proteomes by ^{18}O Labeling. Mol Cell Proteomics. 2011; 10:1–14.10.1074/mcp.M1110.003335

51. Carroll JS, Meyer CA, Song J, Li W, Geistlinger TR, Eeckhoute J, Brodsky AS, Keeton EK, Fertuck KC, Hall GF, Wang QB, Bekiranov S, Sementchenko V, Fox EA, Silver PA, Gingeras TR, Liu XS, Brown M. Genome-wide analysis of estrogen receptor binding sites. Nat Genet. 2006; 38:1289–1297. [PubMed: 17013392]

52. Millevoi S, Loulergue C, Dettwiler S, Karaa SZ, Keller W, Antoniou M, Vagner S. An interaction between U2AF 65 and CF I(m) links the splicing and 3′ end processing machineries. EMBO J. 2006; 25:4854–4856. [PubMed: 17024186]

53. Kerkhoff C, Klempt M, Sorg C. Novel insights into structure and function of MRP8 (S100A8) and MRP14 (S100A9). BBA-Mol Cell Res. 1998; 1448:200–211.

54. Naranjo V, Villar M, Martin-Hernando MP, Vidal D, Hofle U, Gortazar C, Kocan KM, Vazquez J, de la Fuente J. Proteomic and transcriptomic analyses of differential stress/inflammatory responses in mandibular lymph nodes and oropharyngeal tonsils of European wild boars naturally infected with Mycobacterium bovis. Proteomics. 2007; 7:220–231. [PubMed: 17163576]

55. Kimura Y, Yokoyama R, Ishizu Y, Nishigaki T, Murahashi Y, Hijikata A, Kitamura H, Ohara O. Construction of quantitative proteome reference maps of mouse spleen and lymph node based on two-dimensional gel electrophoresis. Proteomics. 2006; 6:3833–3844. [PubMed: 16767787]

56. Leak LV, Liotta LA, Krutzsch H, Jones M, Fusaroa VA, Ross SJ, Zhaos YM, Petricoin EF. Proteomic analysis of lymph. Proteomics. 2004; 4:753–765. [PubMed: 14997497]

57. Shriver C, Sullivan A, Somiari S, Russell S, Heckman C, Hooke J, Somiari RI. Proteomics analysis of breast tumors and lymph nodes by 2-dimensional differential in-gel electrophoresis. Ann Surg Oncol. 2003; 10:S15–S15.

58. Antonucci F, Chilosi M, Santacatterina M, Herbert B, Righetti PG. Proteomics and immunomapping of reactive lymph-node and lymphoma. Electrophoresis. 2002; 23:356–362. [PubMed: 11840544]

59. Manolova V, Flace A, Bauer M, Schwarz K, Saudan P, Bachmann MF. Nanoparticles target distinct dendritic cell populations according to their size. Eur J Immunol. 2008; 38:1404–1413. [PubMed: 18389478]

60. Choi HS, Ashitate Y, Lee JH, Kim SH, Matsui A, Insin N, Bawendi MG, Semmler-Behnke M, Frangioni JV, Tsuda A. Rapid translocation of nanoparticles from the lung airspaces to the body. Nat Biotech. 2010; 28:1300–1303.

61. Bhardwaj RS, Zotz C, Zwadloklarwasser G, Roth J, Goebeler M, Mahnke K, Falk M, Meinardushager G, Sorg C. The calcium-binding proteins MRP8 and MRP14 form a membrane-associated heterodimer in a subset of monocytes/macrophages present in acute but absent in chronic inflammatory lesions. Eur J Immunol. 1992; 22:1891–1897. [PubMed: 1378023]

62. Rosen ED, Spiegelman BM. PPAR gamma: a nuclear regulator of metabolism, differentiation, and cell growth. J Biol Chem. 2001; 276:37731–37734. [PubMed: 11459852]

63. Nielsen R, Pedersen TA, Hagenbeek D, Moulos P, Siersbaek R, Megens E, Denissov S, Borgesen M, Francoijs KJ, Mandrup S, Stunnenberg HG. Genome-wide profiling of PPAR gamma:RXR and RNA polymerase II occupancy reveals temporal activation of distinct metabolic pathways and changes in RXR dimer composition during adipogenesis. Gene Dev. 2008; 22:2953–2967. [PubMed: 18981474]

64. Gearhart J, Pashos EE, Prasad MK. Pluripotency redux - Advances in stem-cell research. New Engl J Med. 2007; 357:1469–1472. [PubMed: 17928593]
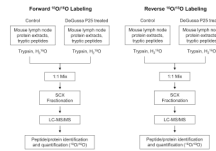
Figure 1.
Schematic flowcharts of forward and reverse trypsin-catalyzed $^{16}O/^{18}O$ labeling combined with SCX fractionation and LC-MS/MS for comparative analysis of proteome changes in lymph nodes from DeGussa P25 TiO$_2$ nanoparticle-treated *vs* control mice.
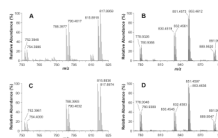
Figure 2.
MS spectra showing complete trypin-catalyzed [18]O labeling. Three and four major pairs of peptides at LC elution time of approximately 25 min (A) and 38 min (B), respectively, were detected in the defined mass ranges from a fraction of forward ^{18}O-labeled sample. The corresponding peaks of the same peptides from the reverse labeling are shown in C and D, respectively.
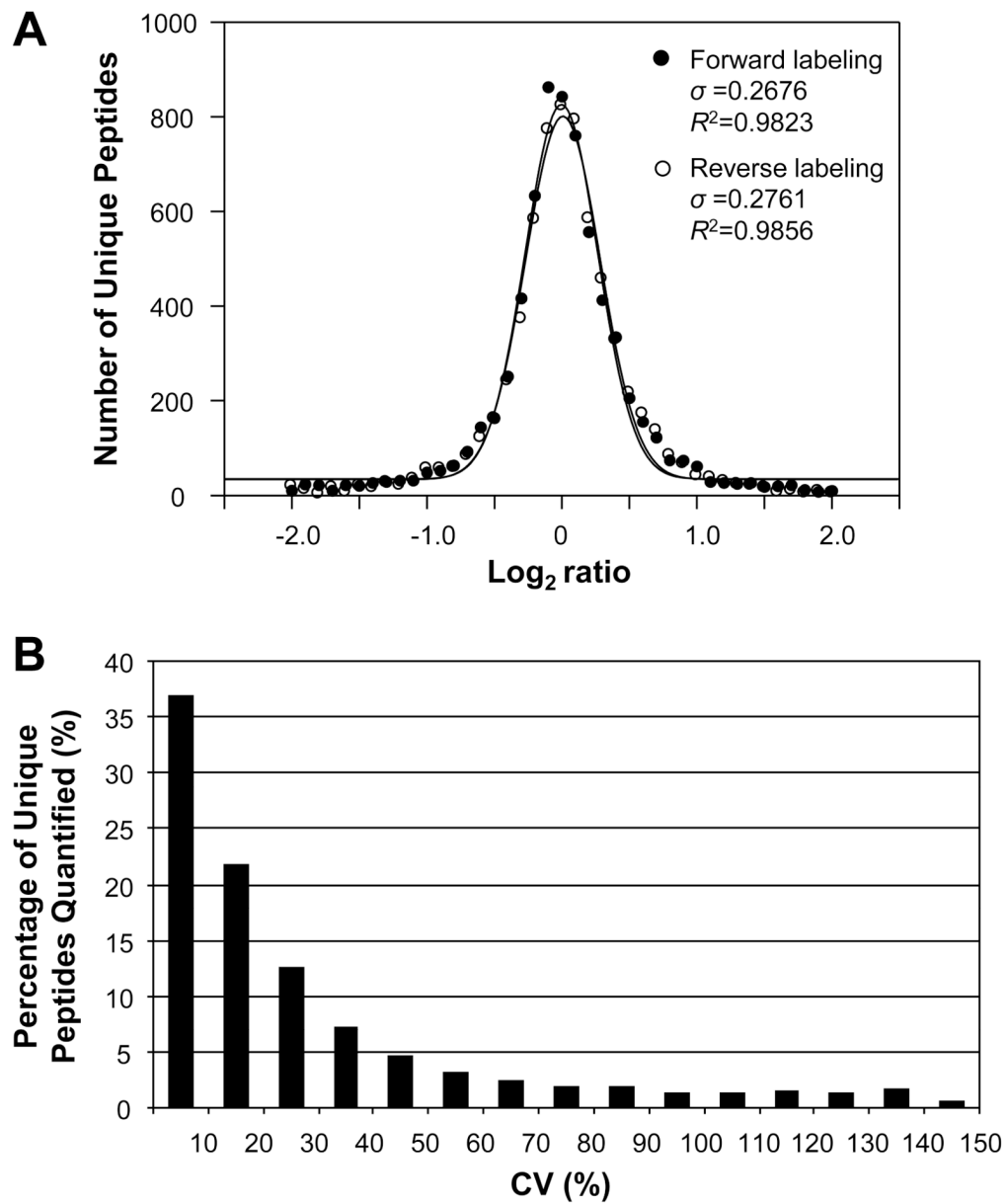
Figure 3.
A) Normal distribution of the 7030 common unique peptides quantified from both forward and reverse ^{18}O labeling experiments within binned base 2 logarithms of peptide abundance ratios. An average ratio was calculated if a peptide was identified and quantified multiple times. B) Plot of relative number of peptides (%) versus binned coefficient of variation (CV) of abundance ratios for the 7030 common unique peptides quantified from both forward and reverse ^{18}O labeling experiments. The CV of a peptide was calculated for its ratios obtained from forward and reverse ^{18}O labeling analyses, indicating the ratio variance between forward and reverse labeling.
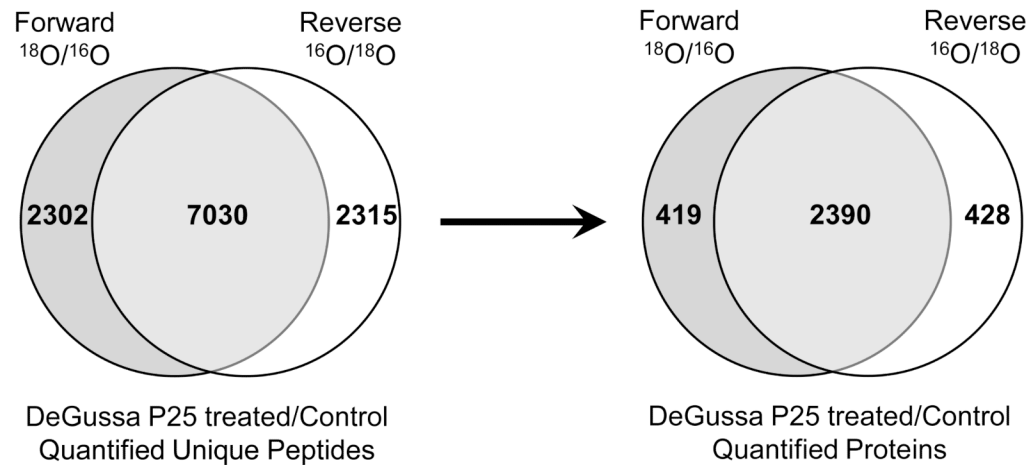
Figure 4.
Venn diagrams showing the number of unique peptides (left) and proteins (right) as well as their overlaps identified from forward and reverse trypsin-catalyzed $^{16}O/^{18}O$ labeling analyses.
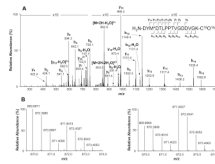
Figure 5.
Identification and quantitative comparison of the peptide DYM*DTLPPTVGDDVGK from cleavage and polyadenylation specificity factor subunit 6 (CPSF6). (A) MS/MS spectrum of the ^{18}O-labeled version of this peptide. (B) MS spectra of the doubly charged peptide pairs showing the relative abundance of this peptide as a result of forward (left) and reverse (right) ^{18}O-labeling. Consistent abundance ratios between the forward (^{18}O/^{16}O=0.63) and reverse (^{16}O/^{18}O=0.70) labeling indicate down-regulation of CPSF6 in the mouse lymph nodes due to DeGussa P25 TiO$_2$ nanoparticle treatment. * indicates the oxidized methionine residue in the peptide.
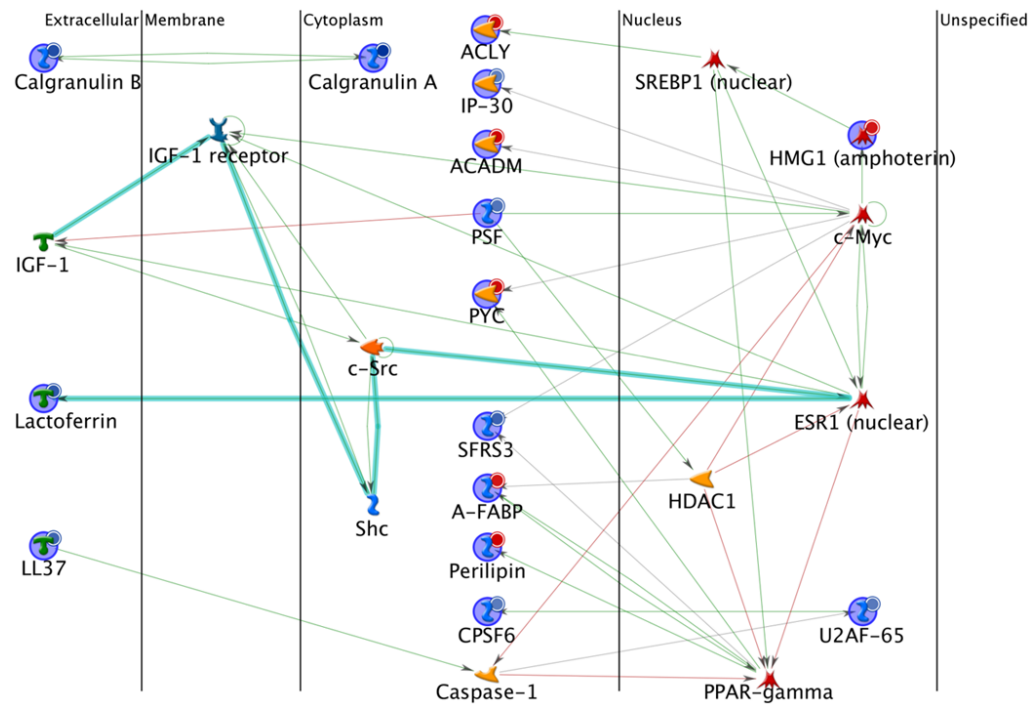
Figure 6.
Protein interaction network of differentially expressed lymph node proteins between the
DeGussa P25 TiO$_2$ nanoparticles treated and the control mice. Network analysis was
performed using the MetaCore program via the shortest paths algorithm for all the 33
differentially expressed proteins. As a result, 15 proteins were included in this map. The
lines between the gene (protein) symbols show different effects between up- and down-
streams: inhibition (pink lines), activation (green lines), unspecified (grey lines) and
fragments of canonical pathways (thick cyan lines). Up-regulated proteins are marked with
red circles and down-regulated with blue circles.

Table 1

Proteins showing statistically significant change in their expression (≥1.3-fold change and $p<0.05$) in mouse lymph nodes at 24 hours after DeGussa P25 TiO$_2$ nanoparticles treatment as revealed from trypsin-catalyzed $^{16}O/^{18}O$ labeling analysis.

Accession	Gene	Description	Subcellular Localization	Forward $^{18}O/^{16}O$ Label (P25/Control)			Reverse $^{16}O/^{18}O$ Label (P25/Control)			Biological Function
				Total Peptide Count	Fold Change	p value	Total Peptide Count	Fold Change	p value	
IPI00118173.1	Aoc3	Isoform 1 of Membrane primary amine oxidase	Plasma Membrane	17	1.38	4.35E-05	11	1.63	1.29E-03	Amine metabolism, cell adhesion, inflammatory response
IPI00122475.2	Camp	Cathelin-related antimicrobial peptide (LL37)	Secreted	10	-2.43	1.99E-20	8	-2.84	3.32E-12	Antimicrobial activity
IPI00317340.1	Ltf	Lactotransferrin	Secreted	4	-3.50	8.29E-03	3	-2.81	3.35E-02	Antimicrobial activity, iron transport
IPI00230768.5	S100a8	Protein S100-A8 (Calgranulin A)	Cytoplasm	4	-2.38	4.38E-05	6	-5.46	4.29E-09	Immune response, antimicrobial, chemotaxis
IPI00222556.5	S100a9	Protein S100-A9 (Calgranulin B)	Cytoplasm	2	-4.01	4.96E-02	2	-4.06	1.07E-02	Inflammation, antimicrobial, chemotaxis
IPI00157508.2	Chi3l3	Chitinase-3-like protein 3	Secreted	9	-2.55	8.38E-07	15	-1.67	7.98E-10	Inflammatory response
IPI00223783.2	Plin1	Isoform 1 of Perilipin-1	Cytoplasm	12	1.70	2.52E-03	9	1.71	5.33E-03	Lipid metabolism
IPI00132874.4	Mgll	Monoglyceride lipase	Plasma Membrane	5	1.35	5.34E-08	12	1.43	2.93E-06	Lipid metabolism, fatty acid biosynthesis
IPI00454049.4	Echs1	Enoyl-CoA hydratase, mitochondrial	Cytoplasm	11	1.38	5.88E-05	9	1.38	1.67E-03	Lipid metabolism, fatty acid metabolism
IPI00134961.1	Acadm	Medium-chain specific acyl-CoA dehydrogenase, mitochondrial	Cytoplasm	8	1.55	1.76E-05	10	1.67	3.93E-15	Lipid metabolism, fatty acid metabolism
IPI00126248.3	Acly	ATP-citrate synthase, mitochondrial	Cytoplasm	72	1.38	6.34E-13	57	1.39	1.72E-11	Lipid synthesis, carbohydrate metabolism
IPI00421241.5	Acacb	Acetyl-Coenzyme A carboxylase beta	Cytoplasm	8	1.60	1.23E-08	8	1.59	2.36E-03	Lipid synthesis, fatty acid biosynthesis
IPI00114710.3	Pcx	Pyruvate carboxylase, mitochondrial (PYC)	Cytoplasm	53	1.57	2.03E-15	36	1.53	6.70E-18	Lipid synthesis, gluconeogenesis
IPI00116705.5	Fabp4	Fatty acid-binding protein, adipocyte (A-FABP)	Cytoplasm	37	1.42	3.56E-10	24	1.32	3.29E-02	Lipid transport
IPI00421085.1	Cpsf6	Cleavage and polyadenylation specificity factor subunit 6	Nucleus	9	-1.59	4.30E-03	13	-1.38	2.22E-02	mRNA processing
IPI00122418.1	Luc7l3	Isoform 2 of Luc7-like protein 3	Nucleus	3	-1.31	3.02E-04	4	-1.41	6.52E-05	mRNA processing, apoptosis, stress response
IPI00129430.1	Sfpq (PSF)	Splicing factor, proline- and glutamine-rich	Nucleus	26	-1.79	1.80E-12	33	-1.98	1.30E-09	mRNA processing, DNA repair, transcription regulation
IPI00129323.1	Srsf3 (Sfrs3)	Isoform Long of Serine/arginine-rich splicing factor 3	Nucleus	4	-2.90	4.46E-02	9	-1.71	6.17E-06	mRNA processing, mRNA splicing
IPI00113746.3	U2af2	Splicing factor U2AF 65 kDa subunit (U2AF-65)	Nucleus	9	-1.67	1.27E-05	7	-1.70	1.13E-08	mRNA processing, mRNA splicing
IPI00121135.5	Srsf2	Serine/arginine-rich splicing factor 2	Nucleus	15	-1.47	5.61E-10	25	-1.40	7.91E-36	mRNA processing, mRNA splicing
IPI00468896.7	Ddx46	Isoform 1 of Probable ATP-dependent RNA helicase DDX46	Nucleus	12	-1.38	1.57E-07	15	-1.81	1.74E-10	mRNA processing, mRNA splicing
IPI00329998.3	Hist1h4a	Histone H4	Nucleus	52	1.46	2.03E-32	38	1.62	2.73E-14	Nucleosome assembly

Accession	Gene	Description	Subcellular Localization	Forward ^{18}O/^{16}O Label (P25/Control)			Reverse ^{16}O/^{18}O Label (P25/Control)			Biological Function
				Total Peptide Count	Fold Change	p value	Total Peptide Count	Fold Change	p value	
IPI00114642.4	Hist1h2bm; Hist1h2bj;Hist1h2bj;Hist1h2bf	Histone H2B type 1-F/J/L	Nucleus	18	1.33	6.23E-09	22	1.43	2.51E-16	Nucleosome assembly
IPI00153400.2	H2afj	Histone H2A.J	Nucleus	12	1.54	1.63E-10	9	1.62	3.40E-02	Nucleosome assembly
IPI00223713.5	Hist1h1c	Histone H1.2	Nucleus	14	1.73	2.90E-09	12	2.29	1.85E-04	Nucleosome assembly, nucleosome positioning
IPI00474959.2	Rcn2	Reticulocalbin 2	Cytoplasm	2	-2.53	6.57E-04	2	-1.66	2.55E-04	Calcium ion binding
IPI00113886.1	Lmnb2	Isoform B3 of Lamin-B2	Nucleus	9	1.48	3.55E-04	4	1.55	5.68E-04	Component of nuclear membrane, structural molecule activity
IPI00420261.5	Hmgb1 (Hmg1)	High mobility group protein B1 (Amphoterin)	Nucleus	34	1.35	1.67E-10	36	1.41	8.49E-10	DNA repair, DNA ligation, DNA recombination, apoptosis
IPI00109044.8	2900073G1 5Rik	Myosin light chain, regulatory B-like	Cytoplasm	20	1.45	5.90E-15	14	1.43	4.37E-09	Motor activity
IPI00114894.1	Myh11	Isoform 1 of Myosin-11	Cytoplasm	22	1.46	2.15E-05	15	2.16	2.14E-03	Motor activity
IPI00113659.4	Ifi30	Interferon gamma inducible protein 30 (IP-30)	Cytoplasm	4	-1.30	4.62E-03	9	-1.32	3.17E-05	Oxidoreductase activity
IPI00352984.4	Xdh	Xanthine dehydrogenase/oxidase	Cytoplasm	15	1.48	4.32E-07	11	1.45	3.16E-08	Oxidoreductase activity
IPI00116222.1	Hibadh	3-hydroxyisobutyrate dehydrogenase, mitochondrial	Cytoplasm	18	1.46	1.92E-03	13	1.38	4.09E-09	Valine metabolism, pentose-phosphate shunt

Table 2

Top five Gene Ontology (GO) processes involved by the differentially expressed proteins. GO processes were ranked by the number of genes linked to the corresponding GO process.

Gene Ontology (GO) Process	Number of Genes	Gene	p value
Response to stimulus	20	S100a8, S100a9, Ltf, Camp, Chi3l3, Xdh, Acacb, Aoc3, Mgll, Ifi30, Acadm, Sfpq, Pcx, Srsf3, Fabp4, Plin1, Luc7l3, Hmgb1, U2af2, Hist1h2bn/Hist1h2bj/Hist1h2bl/Hist1h2bf	9.21E-07
Response to stress	17	S100a8, S100a9, Ltf, Camp, Chi3l3, Aoc3, Mgll, Acadm, Sfpq, Pcx, Srsf3, Fabp4, Plin1, Luc7l3, Hmgb1, U2af2, Hist1h2bn/Hist1h2bj/Hist1h2bl/Hist1h2bf	5.94E-08
Response to organic substance	14	S100a8, S100a9, Ltf, Camp, Acacb, Ifi30, Acadm, Sfpq, Pcx, Srsf3, Fabp4, Plin1, Hmgb1, U2af2	3.26E-07
Multi-organism process	13	S100a8, S100a9, Ltf, Camp, Ifi30, Acadm, Sfpq, Pcx, Srsf3, Fabp4, Hmgb1, U2af2, Hist1h2bn/Hist1h2bj/Hist1h2bl/Hist1h2bf	4.66E-07
Cellular response to chemical stimulus	12	S100a8, S100a9, Ltf, Camp, Ifi30, Acadm, Sfpq, Pcx, Srsf3, Fabp4, Plin1, Hmgb1	5.52E-07